MOLECULAR AND CELLULAR BIOLOGY, Aug. 2005, p. 7193–7202 Vol. 25, No. 16
0270-7306/05/$08.00+0 doi:10.1128/MCB.25.16.7193–7202.2005

Rybp/DEDAF Is Required for Early Postimplantation and for Central Nervous System Development

Melinda K. Pirity,[1] Joseph Locker,[2] and Nicole Schreiber-Agus[1]*

Department of Molecular Genetics[1] and Department of Pathology,[2] Albert Einstein College of Medicine, 1300 Morris Park Avenue, Bronx, New York 10461

Received 4 February 2005/Returned for modification 26 April 2005/Accepted 1 June 2005

The Rybp/DEDAF protein has been implicated in both transcriptional regulation and apoptotic signaling, but its precise molecular function is unclear. To determine the physiological role of Rybp, we analyzed its expression during mouse development and generated mice carrying a targeted deletion of Rybp using homologous recombination in embryonic stem cells. Rybp was found to be broadly expressed during embryogenesis and was particularly abundant in extraembryonic tissues, including trophoblast giant cells. Consistent with this result, *rybp* homozygous null embryos exhibited lethality at the early postimplantation stage. At this time, Rybp was essential for survival of the embryo, for the establishment of functional extraembryonic structures, and for the execution of full decidualization. Through the use of a chimeric approach, the embryonic lethal phenotype was circumvented and a role for Rybp in central nervous system development was uncovered. Specifically, the presence of Rybp-deficient cells resulted in marked forebrain overgrowth and in localized regions of disrupted neural tube closure. Functions for Rybp in the brain also were supported by the finding of exencephaly in about 15% of *rybp* heterozygous mutant embryos, and by Rybp's distinct neural expression pattern. Together, these findings support critical roles for Rybp at multiple stages of mouse embryogenesis.

During development, signaling pathways and transcription factors orchestrate patterns of gene expression to control cellular processes including proliferation, differentiation, apoptosis, and migration. The Rybp protein (for *R*ing1 and *Y*Y1 *b*inding *p*rotein [9], also called DEDAF [33] and YEAF1 [27]), has been linked to some of these processes by virtue of its physical and functional interactions with a variety of relevant proteins. Rybp engages Polycomb group (PcG) proteins, transcriptional corepressors that participate in the establishment of a stably silenced state of key developmental (e.g., *hox*) and proliferation genes (for a recent review, see reference 18). Indeed, Rybp first was cloned as an interactor for Ring1A (Ring1; ortholog of *Drosophila* dRing/Sce) and also was shown to associate with Ring1B (Ring2/Rnf2; ortholog of *Drosophila* dRing/Sce) and M33 (Pc1; ortholog of *Drosophila* Pc) (9). These three PcG members function as components of the PRC1 multiprotein complex that maintains the repressed state of loci that have previously been "marked" for repression via the histone methyltransferase activity of the PRC2 PcG initiation complex (18). Recently, a subset of PRC1 proteins has been shown to function in histone H2A monoubiquitination, this providing a possible molecular basis for PRC1 transcriptional silencing properties (6, 8, 31). Because Rybp can bind to PRC1 proteins as well as to several sequence-specific transcription factors, it has been classified as an adapter protein that can recruit the PcG proteins to these factors and the specific genetic loci they regulate (for examples, see references 9, 27, and 30). As an aside, it has also been proposed that Rybp can serve as a bridging factor between two DNA binding transcription factors (for examples, see references 27 and 28), although it should be noted that one of the partners is often YY1, which itself has been classified as a PcG component (for an example, see reference 1). An Rybp-related protein, Yaf2 (~55% identity on the amino acid level), also has been shown to engage PRC1 components and DNA binding transcription factors (14, 15, 22, 27). One model that has emerged for the Rybp/Yaf2 cofactor family is that Rybp participates in transcriptional corepression and Yaf2 in transcriptional coactivation (9, 14, 27); however, the converse has been reported as well (for examples, see references 19 and 28).

In addition to this putative role in transcriptional regulation, Rybp has been described as a positive regulator of apoptosis (in the apoptotic context, Rybp is known as DEDAF, for *d*eath *e*ffector *d*omain [DED]-*a*ssociated *f*actor). In one report, Rybp was shown to bind nonhomotypically to DED-containing apoptotic mediators (i.e., the cytoplasmic FADD, procaspase 8, procaspase 10, and the nuclear DEDD) and to enhance apoptosis mediated by the death receptors as well as by the DEDs themselves (33). In a second report, Rybp was shown to associate with the viral apoptosis agonist Apoptin. Having a profile similar to that of Apoptin, Rybp was able to promote caspase-dependent apoptosis when overexpressed in the transformed but not the normal cell lines tested (5). Finally, it has been suggested that the intrinsic capacity of Rybp to induce apoptosis may relate to its putative ability to elicit repression of relevant genetic targets (5).

To investigate the biological role of the multifunctional Rybp protein, we have analyzed Rybp expression patterns in developing mouse embryos and targeted Rybp for deletion in the mouse using homologous recombination in embryonic stem (ES) cells. *rybp* homozygous null embryos initiate implantation but fail to undergo complete decidualization and succumb to lethality around embryonic day 5.5 (E5.5) to E6.0. In a subset of heterozygous animals and in $rybp^{-/-} \leftrightarrow rybp^{+/+}$ chi-

* Corresponding author. Mailing address: 1300 Morris Park Avenue, Ullmann 809, Bronx, NY 10461. Phone: (718) 430-3216. Fax: (718) 430-8778. E-mail: agus@aecom.yu.edu.

meras, reduced Rybp levels lead to dramatic perturbations in neurulation and the normal morphogenesis of the central nervous system. Our findings provide the first demonstration of the integral role of Rybp in mammalian development, both at the early postimplantation stage and during organogenesis.

MATERIALS AND METHODS

Construction of the *rybp* targeting vector. A full-length murine *rybp* cDNA cloned by reverse transcription-PCR (R. Arrigoni, J. Blanck, and N. Schreiber-Agus, unpublished data) was used to probe a mouse 129/SvJ genomic library (Stratagene), identifying an 18-kb *rybp* genomic clone (pRYBP18) that contained exons 3 to 5. Genomic subfragments from pRYBP18 were subcloned into pBluescript SK(+) (Stratagene), and the restriction map and the intron-exon boundaries were determined by direct sequencing and restriction site mapping. To construct the targeting vector, a 5-kb fragment containing a portion of exon 3 and exons 4 and 5 was replaced by an enhanced yellow fluorescent protein (EYFP) reporter followed by a floxed PGKneo cassette; this was flanked by a total of 6 kb of homology (0.75 kb of 5′ homology and 5.25 kb of 3′ homology). The 5′ homology arm was generated by PCR on the pRYBP18 template with primers containing HindIII sites (primer A, 5′-GTTAAGCTTACGCGTTGTGCAGAA ATATTG-3′, and primer B, 5′-GTTAAGCTTCGATGCGAGGTTTCCTACA AC-3′). The PCR product was then cloned in-frame with the fluorescent reporter in an EYFP (Clontech)-floxed neo vector (kind gift of K. Hadjantonakis). For the 3′ homology arm, a 5.25-kb HindIII fragment distal to the 3′ untranslated region (UTR) of *rybp* was cloned into a SacII site situated after the floxed pGK-Neo cassette. The targeting vector was linearized with Mlu1 (introduced via primer A) and electroporated into R1 ES cells (21). Further details of targeting vector construction are available upon request.

Generation and characterization of heterozygous null ES cell lines. R1 ES cells were cultured as described previously (21). Following electroporation with the targeting vector, clones resistant to G418 (200 μg/ml concentration; Gibco) were selected, and homologous recombination events were identified by Southern blotting and PCR on genomic DNA prepared as described previously (21, 24). For the Southern blotting, DNA was digested with Xba1, electrophoresed, blotted onto nylon membranes, and hybridized with a [α-^{32}P]dCTP 0.35-kb fragment from intron 2. This probe was generated by PCR on pRYBP18 using primer A (5′-CAAACCCTATCTCGGGTTGCA-3′) and primer B (5′-GGGT ACAATGCGAGGACAGTT-3′) and detected an 8.0-kb wild-type Xba1 fragment and a 5-kb Xba1 fragment in properly targeted clones. For the genomic PCRs, the *rybp* intron 2 primer A (5′-TATGGCTACACGATATGGGCT-3′) and the EGFP-N sequencing primer (Clontech) were used for amplification with 33 cycles of 94°C for 40 s, 60°C for 30 s, and 72°C for 120 s, producing an 800-bp fragment from the correctly targeted allele.

Generation of *rybp* mutant mouse lines and genotyping. Three correctly targeted heterozygous ES cell clones (A6, F4, and G1) were injected into C57BL/6 blastocysts and produced germ line chimeras. Male chimeras were mated with ICR or CD1 females, and their agouti offspring were tested for transmission by PCR on genomic tail DNA with primers described above as well as with primers that amplify YFP (primer A, 5′-AAGTTCATCTGCACCACCG-3′, and primer B, 5′-TGCTCAGGTAGTGGTTGTCG-3′).

Animals heterozygous for the targeted allele were intercrossed, and over 1,000 offspring were analyzed for the three lines on the mixed (129 × ICR) background. All three lines exhibited the same mutant phenotypes. Mice were kept on a 12-h light–12-h dark cycle and maintained in the barrier facility at AECOM in accordance with institutional and federal guidelines.

Production of *rybp*$^{-/-}$ ES cells. To generate *rybp* double-knockout ES cell lines, the PGKneo cassette was removed by electroporating two of the heterozygous null ES cell clones (A6 and F4) with 25 μg of a cytomegalovirus-Cre-recombinase expression plasmid (pBS185) (26). Two days after electroporation, cells were replated at low density (5×10^4 ES cells/10-mm tissue culture dishes with gelatin), allowing them to form single colonies. Five days later, single colonies were picked, expanded, replica plated, and analyzed for the excision event. Excised clones were identified based on acquired G418 sensitivity (200 μg/ml for 7 to 9 days; Gibco) and by PCR on genomic DNA. For the latter, the following primers were used to assess the presence/absence of PGKneo: primer A, 5′-AGAGGCTATTCGGCTATGACTG-3′, and primer B, 5′-CCTGATCG ACAAGACCGGCTTC-3′. As a positive control for the PCR, the following primers were used to amplify a genomic fragment of mouse *mxi1*: primer A, 5′-CTGGTGTTTCTTCTGGCTTCC-3′, and primer B, 5′-GGGGCTCGGCAT GGAGGGGAA-3′). Clones that were negative for a 0.15-kb PCR product for the PGKneo reactions but positive for the control reactions were chosen for the next electroporation, wherein the original targeting vector was reintroduced. DNA was extracted from the retargeted G418-resistant clones and screened by Southern blotting analysis or PCR as described above.

Western blotting analysis. ES cells were washed with phosphate-buffered saline (PBS) and lysed in ice-cold modified radioimmunoprecipitation assay buffer (1% NP-40, 1% deoxycholic acid, 0.1% sodium dodecyl sulfate, 150 mM NaCl, 10 mM sodium phosphate [pH 7.2], 2 mM EDTA, and 50 mM Tris-HCl, in the presence of proteinase inhibitors). Aliquots (10 μg) of cleared lysates were fractionated on a 10% sodium dodecyl sulfate-polyacrylamide gel and analyzed by Western blotting by incubating membranes overnight with the anti-RYBP (anti-DEDAF; 1:1,000, Chemicon AB3637), anti-Max (1:1,000, Santa Cruz SC-197) or anti-GFP (1:1,000, Molecular Probes A11122) primary antibodies. Membranes were then probed with a 1:5,000 dilution of the horseradish peroxidase-conjugated anti-rabbit secondary antibody (NA934V; Amersham), and detection was by chemiluminescence (ECL kit; Amersham).

Histology and immunohistochemistry. Embryos were fixed overnight in fresh buffered 4% paraformaldehyde, and paraffin-embedded sections (6 μm) were mounted for staining. For immunohistochemistry, deparaffinized and rehydrated tissue slides were first treated for 30 min with 3% H_2O_2 to inactivate endogenous peroxidases. After rinsing in double-distilled H_2O and soaking in PBS for 5 to 10 min, slides were blocked with 10% (wt/vol) bovine serum albumin in PBS and then exposed at 4°C overnight to the following antibodies: anti-phospho-histone H3 (Ser 10), clone RR002 (mouse monoclonal, 1:1,000; Upstate 05-598MG) and anti-RYBP (rabbit anti-DEDAF polyclonal, 1:100; Chemicon AB3637). After excess antibody was removed from the samples, they were incubated with a 1:400 dilution of biotin-conjugated secondary anti-rabbit or anti-mouse antibodies (Vector labs) for 45 min at room temperature, washed in PBS, and incubated with avidin-biotinylated enzyme complex for 45 min. The reaction was developed with a DAB kit (Vector labs) and monitored by microscopy for the proper exposure.

Cell death assay. For terminal deoxynucleotidyltransferase-mediated dUTP-biotin nick end labeling (TUNEL) analysis (as described in reference 13), embryos or uteri were fixed overnight in 4% formalin, and paraffin-embedded sections (6 μm) were mounted for staining. Sections were preincubated briefly in 1× One-Phor-All (OPA) buffer (Pharmacia Biotech) containing 0.1% Triton X-100. The solution was then replaced with the hybridization solution consisting 1× OPA buffer, 6 μM dATP, 3 μM biotin-UTP (Sigma), 1 μl terminal transferase (TdT; Pharmacia), and 0.1% Triton X-100 in total volume of 100 μl and incubated at 37°C for 1 h. After being washed with PBS, slides were incubated with Texas Red-coupled streptavidin (1:150 dilution; Calbiochem), in PBS for 30 min at 4°C. Slides were then washed three times in PBS, with 4′,6′-diamidino-2-phenylindole (DAPI) being added to the final wash. Coverslips were applied, and samples were viewed and photographed under epifluorescent illumination with an Axiovert 200M microscope.

Blastocyst outgrowth assay. Heterozygous intercrosses were performed and blastocysts were flushed from uteri at 3.5 days postcoitum; four separate litters were analyzed. Blastocysts were cultured individually on gelatin (Sigma) in 12-well dishes in ES medium, assessed by microscopy, and photographed over a 4-day period. Blastocysts normally attached within 48 h, and subsequent outgrowth formation was defined by the observation of a trophectodermal layer spreading from the attached blastocyst.

For genotyping, cells recovered from the blastocysts preplating were lysed in 2 μl of lysis buffer (5 mM dithiothreitol, 0.8% Igepal CA630, and 900 μg/ml proteinase K in double-distilled H_2O). Samples were heated at 65°C for 15 min and 94°C for 15 min prior to PCR with cycling conditions of 95°C for 12 min; 35 cycles at 94°C for 1 min, 60°C for 1 min, and 72°C for 2 min; and a final extension at 72°C for 7 min. The primers for the *rybp* 3′UTR PCR (not present in null embryos) were as follows: primer A, 5′-GCGACATGTCAGCAGTGAATG-3′, and primer B, 5′-GTGTCAAGAATAACTGTCAGGG-3′; for the *rybp* 5′ UTR PCR (control reaction), primers were as follows: primer A, 5′-CAAACCCTAT CTCGGGTTGCA-3′, and primer B, 5′-GGGTACAATGCGAGGACAGTT-3′. Products (220 bp for 3′ UTR reactions and 400 bp for the 5′ UTR reactions) were visualized after gel electrophoresis and ethidium bromide staining. Blastocysts negative for the 3′ UTR and positive for the 5′ UTR PCRs were considered to be nulls.

Chimera production. Chimeric embryos were generated by microinjecting *rybp*$^{-/-}$ R1 ES cells (129/Sv × 129-Cp) into blastocysts derived from wild-type (*rybp*$^{+/+}$) mice (C57BL/6). The injected blastocysts were implanted into surrogate mothers, and embryos were harvested at various gestational stages. Dissected embryos were visualized for chimerism by fluorescent microscopy, photographed, and processed for histology.

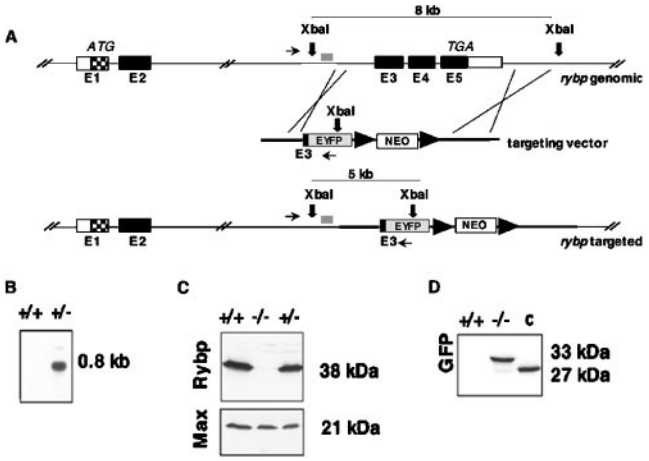

FIG. 1. Targeting of the murine *rybp* gene by homologous recombination. (A) The structure of the mouse *rybp* locus is shown (upper diagram); the targeting vector and disrupted allele are shown in the middle and lower diagrams, respectively. Rectangles represent the five exons (E1 to E5), filled areas represent the Rybp coding region, and unfilled areas represent untranslated regions. The checkered region in exon 1 indicates the 5′ open reading frame of Rybp, whose precise genomic structure remains to be characterized. The double slashes between exon 2 and exon 3 indicate the large size of intron 2 (~53 kb). The location of the start codon (ATG) in exon 1 and the stop codon (TGA) in exon 5 is indicated, along with the diagnostic XbaI restriction enzyme sites and the 5′ probe (gray rectangle) used to detect homologous recombination events by Southern blotting (data not shown). Thin horizontal arrows indicate the locations of primers used in PCRs to detect homologous recombination events. The protein product encoded by the targeted locus is a fusion between the 5′ open reading frame of Rybp (retains amino acids 1 to 58) and the EYFP reporter (Fig. 1D); this fusion protein is likely to be expressed in a pattern that recapitulates endogenous *rybp* gene expression. A floxed PGK-neo cassette (NEO surrounded by triangles) also has been introduced for selection purposes. (B) Southern blot of PCRs performed to identify correctly targeted ES cell clones with the PCR primers shown in panel A. The primers utilized amplify a product of 800 bp that is specific for the homologously recombined locus. The blot was probed with the 5′ probe (gray rectangle in panel A). (C) Immunoblot of total cellular lysates from ES cells probed with affinity-purified antibody directed against the carboxyl-terminal 33 amino acids of Rybp (called anti-DEDAF; Chemicon). An Rybp band of the expected 38-kDa size is present in the $rybp^{+/+}$ sample, slightly reduced in the $rybp^{+/-}$ sample, and absent in the $rybp^{-/-}$ sample. Immunoblotting for the 21-kDa Max protein (anti-Max; Santa Cruz) was performed with the same samples as the loading control. (D) Immunoblot of total cellular lysates from ES cells probed with an anti-GFP antibody (Molecular Probes). An Rybp-YFP fusion protein band of the predicted 33-kDa size is present in the $rybp^{-/-}$ sample and absent in the $rybp^{+/+}$ sample. R1 ES cells stably transfected with GFP were loaded as a control (c) and show the expected 27-kDa GFP protein.

RESULTS

Targeted disruption of *rybp* results in early embryonic lethality. To elucidate the role of Rybp in mouse development, a mutant allele of *rybp* was generated by gene targeting in ES cells and introduced into the mouse germ line. Briefly, genomic clones of the 3′ end of the mouse *rybp* locus were characterized and shown to contain exons 3 to 5 (Fig. 1A) (see Materials and Methods). These exons encode domains that have been shown to mediate key Rybp functions, including its interactions with PRC1 components, various transcription factors, and DED-containing proteins (9, 30, 33), as well as its transcriptional repression activity (9). The targeting vector was designed to deliver a fluorescent reporter (EYFP) into the endogenous locus in-frame with the start of exon 3, while at the same time eliminating the remainder of exon 3 and exons 4 to 5 and introducing a floxed PGK-neo cassette (Fig. 1A) (see Materials and Methods). As shown in Fig. 1C and D, Western blotting analysis of ES cells harboring two targeted *rybp* alleles (homozygous mutant) showed a complete absence of the 38-kDa Rybp protein and the presence instead of the predicted Rybp-YFP fusion protein. Because 75% of the Rybp coding region (including many key functional domains) is absent from this fusion protein, we expect that the normal function of Rybp has been eliminated by the targeting event.

TABLE 1. Gross phenotypic and genotypic analysis of staged embryos from *rybp* heterozygous intercrosses[a]

Age	No. with morphology indicated		No. with genotype indicated (%)[b]		
	Normal	Abnormal	+/+	+/−	−/−
E3.5	41	0	13 (33)	22 (56)	4 (10)
E4.5	19	3	6 (27)	13 (59)	3 (14)
E5.5	38	7	ND	ND	ND
E6.5	65	17[c]	17 (22)	48 (62)	12 (16)
E7.5	44	9R	16 (36)	28 (64)	0
E8.5	37	9R	15 (41)	22 (59)	0

[a] R, resorbed; ND, not determined.
[b] %, the ratio of embryos of a given genotype to the total number of embryos genotyped at a given stage, expressed as a percentage.
[c] Of these 17 morphologically abnormal embryos, 12 were genotyped as homozygous null and 5 as heterozygous.

Lines of mice carrying one mutant *rybp* allele were generated from three independently targeted ES cell clones (Fig. 1B), and heterozygous intercrosses were performed. Live-born heterozygous offspring appeared grossly normal, were fertile, and did not show overt signs of ill health (as assessed over a >2-year period of observation). Of note, statistical analysis revealed that the number of live-born *rybp* heterozygotes deviated significantly from the expected Mendelian number (data not shown); indeed, a subset of these animals does not survive beyond birth (see below). Live-born mice homozygous for the disrupted allele were not recovered.

To determine the developmental stage at which the lack of Rybp causes death, litters were dissected at various time points between E7.5 and E18.5 (Table 1 and data not shown). Again, homozygous mutants were not recovered, indicating that the mutation was lethal either before or around the time of implantation. For further assessment, blastocysts were isolated from heterozygous intercrosses by flushing uteri at E3.5 and were then individually photographed and genotyped by PCR. The homozygous null *rybp* genotype was represented (Table 1; E3.5), and these blastocysts were indistinguishable from wild-type and heterozygote blastocysts. Having established the period of lethality to be between E3.5 and E7.5, we focused on this developmental window. Morphological analysis suggested that all Rybp-deficient embryos were markedly abnormal by E6.5 and resorbed by E7.5 (Table 1 and data not shown).

The histology of embryos at E5.0 to E5.5 showed that homozygous mutants were retarded in overall growth and patterning (compare Fig. 2e and a); these mutants could be identified by the absence of Rybp immunoreactivity (for example,

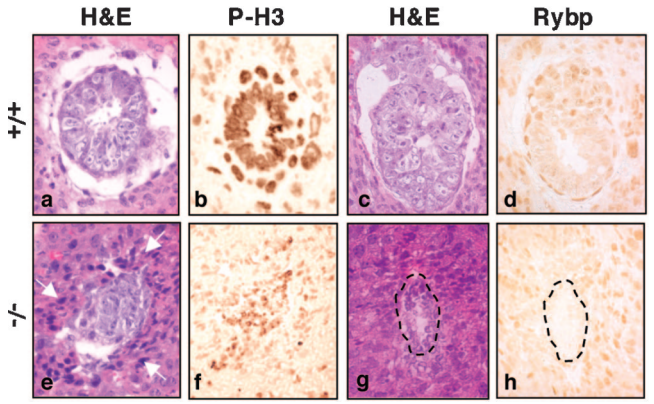

FIG. 2. Impaired viability and morphological characteristics of *rybp*$^{-/-}$ embryos. Representative examples of the histological abnormalities and decreased proliferation in the Rybp-deficient embryos (bottom panels) are shown in comparison to wild-type littermate controls (top panels). Hematoxylin and eosin (H&E) staining of transverse sections of E5.5 embryos is shown in panels a and e, and anti-phosphorylated histone H3 (p-H3) immunohistochemistry is shown on similar sections in panels b and f. The null embryos are growth retarded and lack mitotic activity. Note the imperfect decidual reaction around the mutant embryos in panel e (white arrows). H&E staining of sagittal sections of E6.0 embryos is shown in panels c and g, and anti-Rybp (anti-DEDAF) immunohistochemistry is shown on similar sections in panels d and h. The representative null embryo (outlined) is developmentally arrested and lacks nuclear embryonic and extraembryonic Rybp staining.

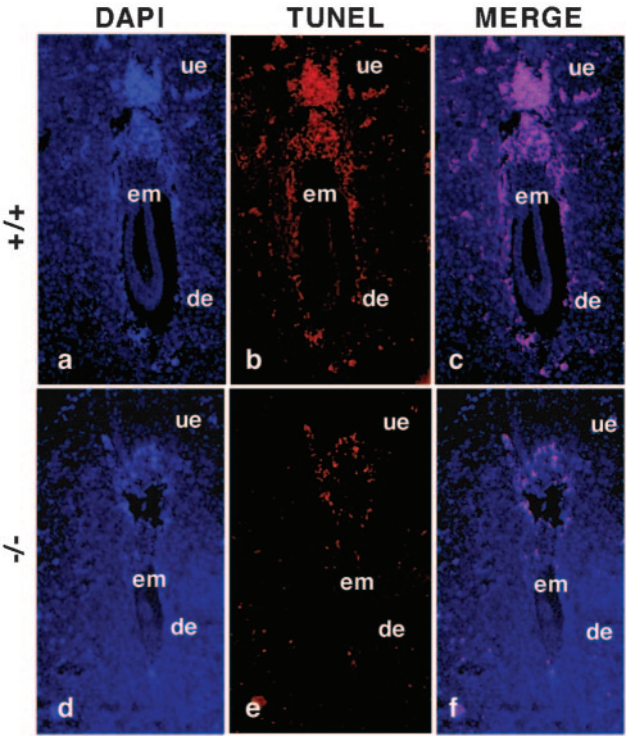

FIG. 3. Lack of apoptosis in the decidua surrounding Rybp-deficient conceptuses. Sagittal sections of *rybp*$^{+/+}$ (a to c) and *rybp*$^{-/-}$ (d to f) embryos and deciduas at E6.0 to E6.5 stained with the nuclear marker DAPI (a and d) and the TUNEL reaction (b and e) are shown; the merge is shown in panels c and f. Note the appearance of TUNEL-positive cells within the deciduas surrounding wild-type embryos and the near lack of the apoptotic decidual reaction for the Rybp-deficient embryos. em, embryo; de, decidual epithelium; ue, uterine epithelium.

compare Fig. 2h and d). In the mutants, the embryonic and extraembryonic layers were indistinguishable, the presumptive epiblast was disorganized, and cellular degeneration was observed. By E6.0, a cylinder-like two-layered cellular structure was observed for the wild-type embryos, with evident embryonic and extraembryonic compartments surrounded by visceral endoderm cells having classical columnar morphology (Fig. 2c). In contrast, the Rybp-deficient embryos lacked such a cylinder-like structure, and cells present at the site of the presumptive visceral endoderm showed extensive vacuolization (Fig. 2g). Moreover, a decreased number of polyploid trophoblast giant cells was noted for the null animals (data not shown). By E7.5, consistent with what was observed morphologically, disorganized embryos were no longer seen, and a number of "empty" decidua examined at high power did not show remnants of the embryo.

Proliferative failure and lack of full decidual reaction in *rybp* null conceptuses. To gain insight into the basis for the developmental arrest of the Rybp-deficient embryos, levels of cell proliferation and apoptosis were examined by phosphohistone H3 (p-H3) staining and a TUNEL assay, respectively (Fig. 2 and 3). In contrast to the significant number of p-H3-positive, mitotically active cells in the wild-type conceptuses, in both embryonic and extraembryonic structures (Fig. 2b), the Rybp-deficient embryos showed dramatically reduced staining at E5.0 and a lack of staining by E6.0 (Fig. 2f and data not shown). With respect to cell death, TUNEL assays showed minimal staining with the wild-type E5.0 to 6.5 embryos, with no apparent differences with the mutant embryos (Fig. 3b and e, em; data not shown). These findings suggest that reduced proliferation but not excessive cell death in the Rybp-deficient early postimplantation embryo likely contributes to the developmental arrest at this stage.

Strikingly, while there was strong positive TUNEL signal surrounding the implanting wild-type E6 to E6.5 embryos, the signal was markedly reduced for the null embryos (compare Fig. 3b and c with Fig. 3e and f; this difference also was observed at E5.5 [data not shown]). The observed TUNEL reactivity of the wild-type sample marks the apoptosis that normally occurs during the implantation process—first the uterine epithelium apoptoses in response to signaling by the blastocyst, and then the decidual cells regress in response to the invasion by the trophectoderm (see reference 11 and the references therein). That the mutant embryos began to undergo implantation is suggested by the facts that decidual swellings were elicited and that implantation sites were detectable by the method of Evans Blue dye injection (data not shown). However, the near lack of TUNEL reactivity for these mutant embryos at the implantation sites (Fig. 3e) indicates that the absence of Rybp compromises the ability of the epiblast and/or trophoblasts to trigger fully the uterine reaction.

To assess further the nature of the developmental defect, E3.5 blastocysts from heterozygous intercrosses were cultured in vitro in a surrogate assay for peri-implantation development (Fig. 4). During days 1 to 4 in culture, the majority of the blastocysts hatched from the zona pellucida and developed

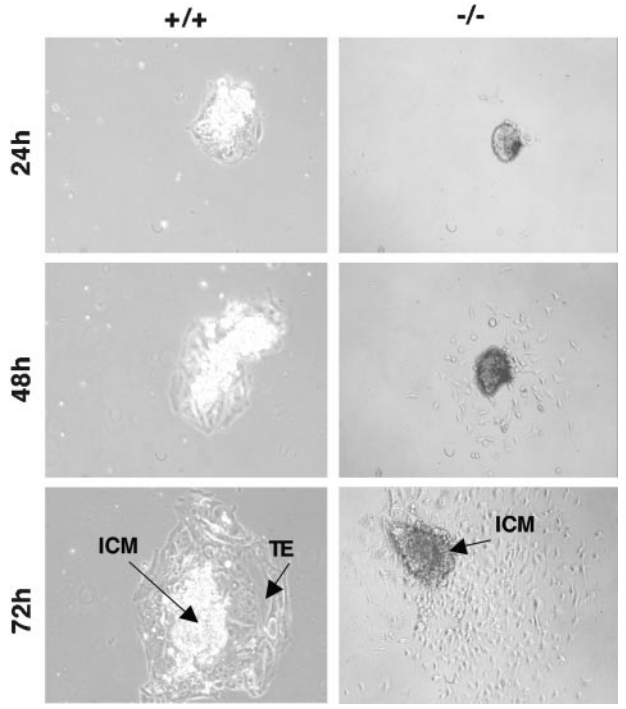

FIG. 4. Failure of Rybp-deficient blastocysts to survive and to yield trophectodermal outgrowths in vitro. *rybp*$^{+/+}$ (left panels) and *rybp*$^{-/-}$ (right panels) blastocysts were cultured for 1 to 4 days (24-, 48-, and 72-h timepoints are shown). Note the proliferating ICM and TE outgrowth layer in the wild-type culture, both of which do not survive in the *rybp*$^{-/-}$ cultures. Genotypes were determined by PCR with cells recovered from the blastocyst preplating.

trophectodermal (TE) outgrowths and proliferating inner cell masses (ICMs) (Fig. 4, left panels [+/+]). In contrast, a subset of the blastocysts failed to survive in vitro or to yield TE; only a few scattered outgrowth cells resembling endoderm were observed (Fig. 4, right panels [−/−]). The genotypes of normal and defective blastocysts were identified by PCR, and the latter group was shown to correlate strictly with the *rybp*$^{-/-}$ genotype. Taken together, our in vitro and in vivo observations suggest that Rybp is required for early postimplantation development.

Localization of Rybp expression in the early embryo. To gain further support for the early embryonic role for Rybp, we determined the Rybp protein expression profile throughout embryogenesis by utilizing a newly developed anti-Rybp (anti-DEDAF) antibody (Chemicon). First, Rybp was shown to be readily detectable in blastocysts and in their ES cell derivatives (Fig. 1C and data not shown). From the beginning of postimplantation development (E5.0 to E5.5), scattered Rybp staining was observed in both the embryonic and extraembryonic compartments, with the latter being more pronounced (data not shown). The prominent extraembryonic Rybp expression persisted during embryogenesis. By E6.0 to 6.5, staining was found in the ectoplacental cone, the extraembryonic ectoderm, the visceral and parietal endoderm (future fetal extraembryonic membranes), and the trophoblast giant cells (Fig. 5a and b; Fig. 2d). This pattern was maintained at later stages in derivatives of these structures, including the chorion (Fig. 5d and e), the allantois (Fig. 5e), the yolk sac (Fig. 5f), and the mature placenta (Fig. 5i). Of note, from E6.0 and beyond, the most intense and reproducible sites of Rybp expression were the trophoblast giant cells, postmitotic polyploid cells that are the first cells to invade the uterus during the process of implantation (Fig. 5h) (for reviews on trophoblast biology and placental development, see references 4 and 25). With respect to the embryo itself from E6.0 to E7.5, specific staining was observed with some cell types, but these cells could not be discriminated histologically from those that were negative for Rybp (Fig. 5a to c); this pattern may suggest that Rybp is differentially expressed throughout the cell cycle. With continued development and organogenesis, a low level of Rybp was observed for many tissues throughout the embryo, with selective upregulation in certain cell types/tissues (e.g., neurons, mesenchyme, and endothelial cells) at various developmental stages (for examples, see Fig. 5g; M. Pirity and N. Schreiber-Agus, unpublished data; and reference 9). Taken together with the phenotypes described above, this expression pattern is consistent with the idea that Rybp is required around the time of implantation for the normal development/function of extraembryonic tissues (e.g., trophectoderm and its derivatives) and possibly also for the embryo proper.

Reduction in Rybp levels interferes with normal central nervous system (CNS) development. To analyze further the developmental potential of cells deficient for Rybp, *rybp*$^{-/-}$ ES cells were generated by sequential targeting and injected into wild-type blastocysts for the production of chimeric embryos (see Materials and Methods). In these chimeras, the epiblast represents a mixture of *rybp*$^{+/+}$ and *rybp*$^{-/-}$ cells, while the primitive endoderm and the trophectoderm are derived entirely from the wild-type host blastocyst (reviewed in reference 29). Moreover, the mutant cells of the embryo proper can be distinguished from the wild-type ones by virtue of the introduced EYFP reporter on both *rybp*-targeted alleles in the mutant cells.

Foster mothers carrying these chimeric embryos were sacrificed at various stages between gestational days 8 and 13.5, and a total of ~50 embryos were dissected and examined morphologically and by fluorescent microscopy. These embryos displayed low levels of chimerism (mostly in the limbs and connective tissue) (Fig. 6b), an observation supported by fluorescence-activated cell sorter analysis of dissociated chimeric embryos, which showed an average of 12% YFP positivity (data not shown). This finding, and the fact that a significant number (~50%) of early resorptions were observed, suggests that high contribution of the deficient ES cells is incompatible with embryonic survival.

Interestingly, a significant proportion of the chimeric embryos harvested at mid-gestation displayed marked CNS malformations (compare Fig. 6d and c). A histological analysis of sections of E11.5 to E13.5 chimeras revealed a range of cephalic abnormalities, including structural disorganization and convolutions, massive hyperplasia, and ectopic neuronal structures, among others. These abnormalities were localized most often to the forebrain, wherein differentiation of the telencephalic and diencephalic vesicles had occurred, but both regions were marked by chaotic overgrowth and invaginations as well as shrunken ventricles (for a representative example, compare Fig. 6f and e). Also observable in the forebrain as well as the

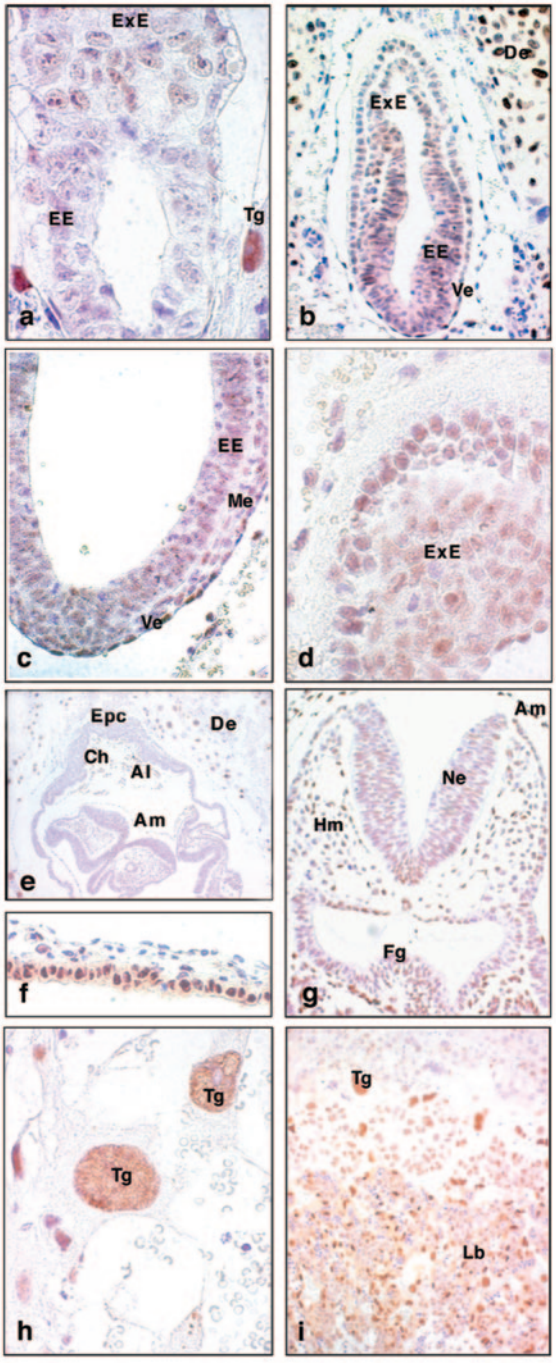

FIG. 5. Early postimplantation expression patterns of Rybp in normal embryos. Representative examples of immunohistochemistries performed with an anti-Rybp (anti-DEDAF; Chemicon) antibody (brown) on counterstained (purple) sections from various stages of postimplantation mouse development (a, E6.0; b, E.6.5; c and d, E7.5; e to h, E8.5; and i, E13.5). (a) E6.0 embryo; mosaic Rybp staining can be seen in all cell layers. (b) E6.5 embryo; note strong expression of Rybp in the trophoblasts and more modest staining of the epiblast and in the visceral endoderm. (c) E7.5 embryo; staining pattern is similar to that for the E6.5 embryo shown in panel b, except that the newly formed mesodermal layer also shows positivity. (d) Extraembryonic portion of an E7.5 embryo showing abundant and almost homogenous expression of RYBP in the chorionic ectoderm. (e) Staining in the allantois and chorion of an E8.5 embryo. (f) Staining in the endodermal lining of the yolk sac of an E8.5 embryo. (g) Head region of an E8.5 embryo showing Rybp expression in the head mesenchyme and in the neuroepithelium of a closing neural plate (see also Fig. 7a). (h) Intensely staining trophoblast giant cells within the decidua surrounding an E8.5 embryo. (i) Strongly stained E13.5 placenta, specifically in the inner labyrinth layer that is chorion plus allantois derived. Of note, Rybp is expressed in the fetal but not maternal compartments of the placenta, and staining is absent in a nonpregnant uterus (data not shown). High-level placental expression of *rybp* transcripts also was reported in references 5 and 33). ExE, extraembryonic ectoderm; EE, embryonic ectoderm; Tg, trophoblast giant cell; De, decidual epithelium; Ve, visceral endoderm; Me, mesoderm; Epc, ectoplacental cone; Ch, chorion; Al, allantois; Am, amnion; Ne, neuroepithelium; Hm, head mesenchyme; Fg, foregut; Lb, labyrinth layer of the placenta.

hindbrain were localized regions of disrupted neural tube closure, although these were unusual in nature in that the overlying surface ectoderm had fused (for a representative example, compare Fig. 6h and g).

The finding that the CNS repeatedly was affected in the chimeras likely reflects the need to maintain the appropriate spatiotemporal expression pattern and levels of Rybp for proper CNS development. This theory also gains support from the observation that a subset (about 15%) of the *rybp* heterozygotes in our conventional knockout colony (all three independent lines) succumbed to death at the time of birth due to exencephaly—exposed, focally hemorrhagic brain masses protruding through open cranial vaults (compare Fig. 6k and i). Histological analysis of exencephalic embryos at E14.5 to E16.5 showed forebrain overgrowth and ventricular stenosis, similar to what was seen with the chimeric animals. Structural displacement/reorganization (e.g., the forebrain appeared to be "buried" under the midbrain) and even the absence of certain structures (e.g., the dorsal aspect of the midbrain/hindbrain, including the cerebellum) were observed as well (compare Fig. 6l and j). The recovery of affected *rybp* heterozygotes from earlier developmental stages allowed us to determine that this "exencephaly" results in part from the failure/disruption of primary neural tube closure in the anterior region (Fig. 6, compare panels o and p with panels m and n). The histology of these open neural tubes revealed both a thickening and a disorganization of the neuroepithelial cells surrounding the affected region (data not shown). In the cranial region of wild-type mice, the process of neural tube closure begins at E8.5 at the hindbrain/cervical boundary (closure 1), continues with closure events at the forebrain/midbrain boundary (closure 2) and the rostral end of the forebrain (closure 3), and is complete by E9.5 (for reviews, see references 3 and 12). The fact that the neural tube is still open (convex) around closure 2 in some E10.5 *rybp* heterozygotes (Fig. 6o and p) suggests that the proper execution of this process is sensitive to Rybp dosage.

Localization of Rybp expression in the developing CNS. As a first attempt to understand the basis for Rybp's integral role in the developing CNS, Rybp protein expression patterns therein were assessed by immunohistochemistry (Fig. 7). At E8.5, modest staining in the pseudostratified neuroepithelial cells of the neural plate was observed, with a specific enrichment in certain cells of the median hinge point (Fig. 7a; also see Fig. 5g). By E10.5, distinct regions of Rybp positivity were observed in neuroblasts of the forebrain (both diencephalon

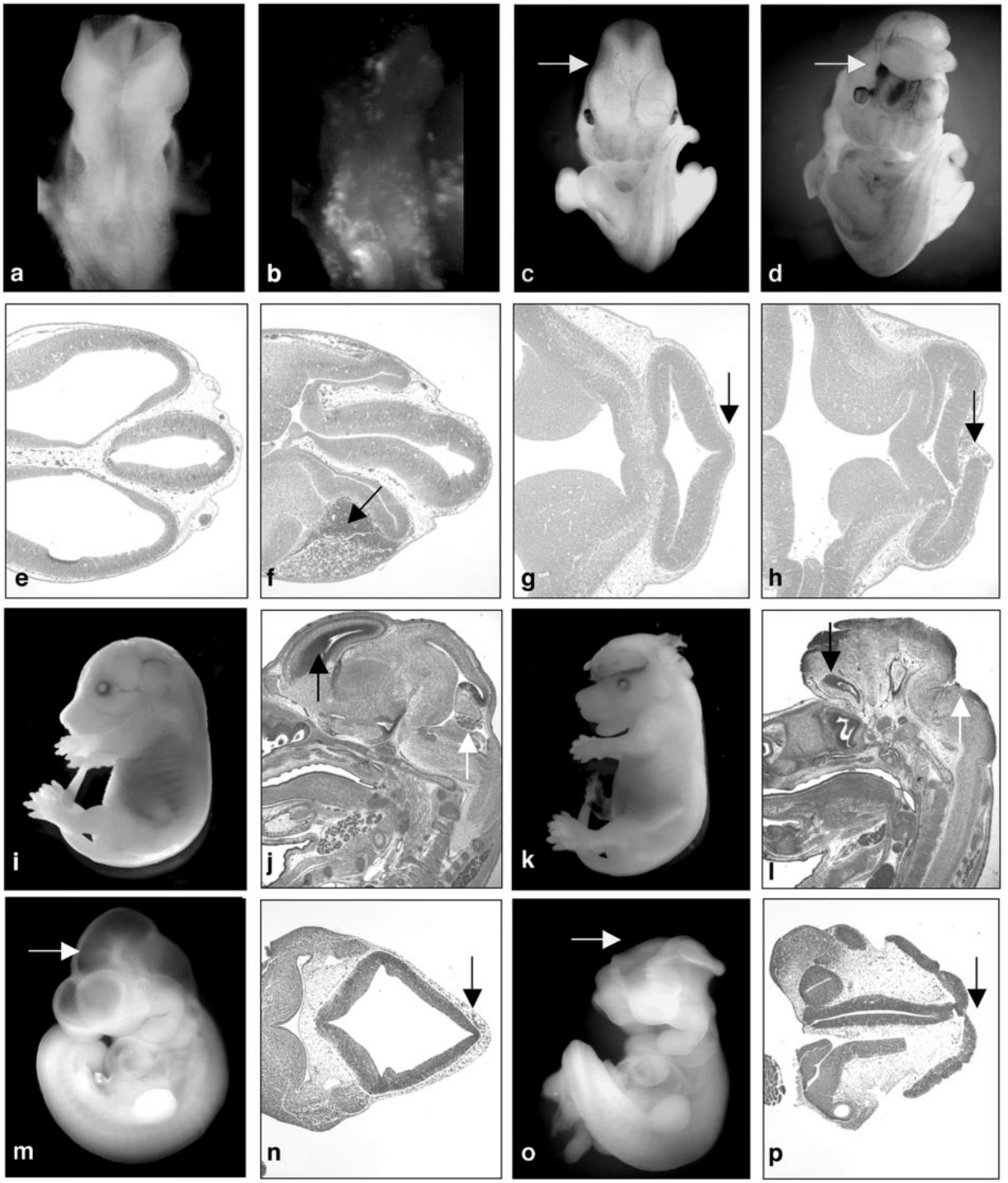

FIG. 6. Reduction in Rybp levels interferes with normal CNS development. (a to h) Malformations selectively in the CNS of *rybp*$^{-/-}$↔*rybp*$^{+/+}$ diploid embryo chimeras. Bright-field (a) and fluorescent (b) microscopic posterior views of a chimeric embryo at E8.5 are shown. The fluorescing cells in panel b are *rybp*$^{-/-}$ ES cell derived; note the weak contribution of these cells to the developing embryo. (c and d) Bright-field views of an E11.5 control and affected chimera, respectively, showing marked forebrain abnormalities and overgrowth (arrows) in the latter. (e to h) Histology of coronal sections of affected chimeric brain (f and h) in comparison to control (e and g). Note the chaotic overgrowth, ventricular stenosis, and hemorrhaging (f, arrow) in the forebrain of the chimera as well as the localized openness of the chimeric neural tube (h, arrow). (i to p) Exencephaly and open neural tube defects in some *rybp* heterozygous null embryos. Representative bright-field views of affected *rybp* heterozygotes (k and o) and wild-type littermate controls (i and m) are shown. Panels i and k show E16.5 embryos; panels m and o show E10.5 embryos. Panels j, l, n, and p show the histology of the corresponding embryos (j, embryo i; l, embryo k; n, embryo m; p, embryo o); panels j and l, sagittal sections; panels n and p, coronal sections. Note the structural displacement/disorganization and ventricular stenosis (black arrows in panels j and l) and the absence of the cerebellum (white arrows in panels j and l) in the affected heterozygote. Note the open (convex) neural tube of the E10.5 *rybp*$^{+/-}$ embryo (panel p compared to panel n, arrows). In the affected heterozygotes, other types of open neural tube defects, including craniorachischisis and spina bifida, were never observed.

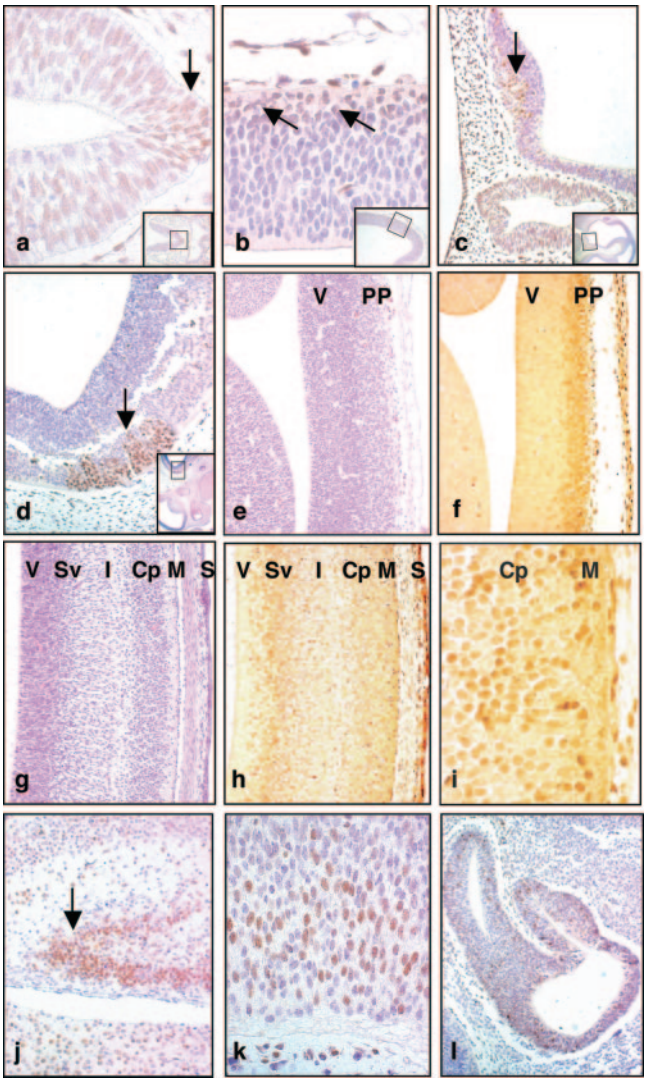

FIG. 7. Expression pattern of Rybp in the developing central nervous system of normal embryos. Representative sites of Rybp expression during various stages of CNS development are shown. Brown staining corresponds to Rybp protein; sections in panels a to d and j to l also were counterstained with hematoxylin and eosin. (a) High-power view of the neuroepithelium of a still-open neural plate in a wild-type E8.5 embryo; a low-power view is shown in the bottom right (and the same embryo is shown in Fig. 5g). The arrow indicates enhanced expression at the median hinge point. (b) Dorsal neopallium of an E10.5 embryo, with arrows showing specific expression of Rybp in the outermost cell layers; a low-power view of the forebrain is shown in the bottom right. (c) Rybp staining in the ventral diencephalon of an E10.0 embryo (arrow). Rybp is also expressed in Rathke's pouch (round structure below); a low-power view is shown in the bottom right. (d) Positively staining isthmus of an E10.5 embryo; a low-power view of this midbrain/hindbrain junction is shown in the bottom right. (e to i) Rybp exhibits a stratified pattern of expression in layers of the mouse neocortex. Panels e and f, H&E-stained and low-power views of anti-Rybp immunohistochemistry, respectively, of an E11.5 neocortex. Note the absence of staining in the ventricular (V) zone and marked staining in the preplate (PP). Panels g to i, H&E-stained and low-power and high-power views of anti-Rybp immunohistochemistry, respectively, of an E16.5 neocortex. Note the absence of staining in the ventricular (V) zone and the strong staining in the cortical plate (Cp) and marginal (M) zones emerged from the preplate. Staining is also apparent in the outer ventricular/subventricular zone. V, ventricular zone; Sv, subventricular zone; I, intermediate zone; PP, preplate; Cp, cortical plate; M, marginal layer; S, skin. (j) Significant and specific Rybp staining in the dentate gyrus of a newborn mouse brain. (k) Rybp positivity in neuroblasts of the spinal cord of an E16.5 embryo. (l) Rybp positivity in the olfactory epithelium of an E11.5 embryo.

and telencephalon) and of the isthmus (junction between midbrain and hindbrain) and the dorsal hindbrain (Fig. 7b to d and data not shown), similar to what has been reported previously for *rybp* mRNA localization during early organogenesis (9). In the cerebral cortex at E11.5 and E12.5, Rybp staining adopted a stratified pattern in which the proliferative ventricular layer was consistently negative, and the postmitotic neurons of the preplate were often positive (Fig. 7e and f; E12.5 not shown). This pattern persisted in the E16.5 cortex, with the cortical plate and marginal zone neurons (derived from the preplate) staining positive, although there was a thin inner layer above the ventricular zone that also showed modest positivity (Fig. 7g to i) (see reference 10 for a review of cerebral cortex formation). Consistent with this result, at the newborn stage, a great many outer cortical neurons of the forebrain and midbrain expressed Rybp, albeit in a mosaic pattern (data not shown). Significant postnatal Rybp expression also was observed in the dentate gyrus of hippocampus (Fig. 7j), in peripheral and cranial nerve ganglia, and in the cephalic mesenchyme (data not shown). Other relevant structures that showed significant Rybp expression during development included the spinal cord (Fig. 7k) and the olfactory epithelium (Fig. 7l). Taken together, these data indicate that Rybp appears to be selectively upregulated in distinct structures and cell types of the developing CNS, and, at least in the cerebral cortex, may play a role in more mature neurons. Of note, several general features of Rybp's neural developmental expression profile are overlapping with that described for the related Yaf2 protein, as assessed by in situ hybridization for *yaf2* with a riboprobe that recognized the known *yaf2* mRNA isoforms collectively (15). Specifically, at the E10.5 to E11.5 stage, *yaf2* transcripts were found in regions of the forebrain and midbrain, the olfactory placodes, various ganglia, the cephalic mesenchyme, as well as the neural tube and migrating neural crest cells of the spinal cord (15). This possible overlap between Rybp and Yaf2 expression obviously was not sufficient to prevent aberrant neurulation/neurogenesis resulting from reduced Rybp levels in our affected heterozygous and chimeric animals (Fig. 6).

DISCUSSION

In the present study, we have addressed the biological role of the multifunctional Rybp protein through the targeted deletion of Rybp in mice. We provide the first genetic evidence for a requirement for Rybp in the early postimplantation period and in CNS development. The phenotypic alterations seen are in accord with the expression pattern of Rybp during embryogenesis.

Rybp-deficient embryos survive the early cleavage and preimplantation periods but succumb to death around E5.5 to E6.0. Survival through the earlier developmental time points likely reflects that Rybp function at these stages is compensated for by maternal Rybp stores or by related proteins or that it is dispensable altogether. At least in ES cells, Rybp defi-

ciency is not cell lethal—doubly targeted ES cells could be recovered, and these cells exhibited proliferative profiles similar to those of their parental controls and were morphologically indistinguishable from these controls by electron microscopy (data not shown). Some degree of compensation may be mediated by Rybp's related family member Yaf2 that has been shown to be expressed in blastocysts (as well as in the early embryo and the placenta) (15). However, around the time of implantation, zygotic Rybp appears to be limiting for embryonic proliferation/survival (Fig. 2). This role also is supported by our in vitro studies showing that *rybp*$^{-/-}$ blastocysts fail to give rise to a surviving ICM component (Fig. 4). Of note, the cultured deficient blastocysts also failed to produce recognizable TE structures, a finding of particular interest in light of the dramatically high level of Rybp expression in trophoblast cells and their derivatives, including the chorion and mature placenta (Fig. 4 and 5). Trophoblast cells are known to play an important role in the implantation process, as they invade the uterine tissue and help to establish the hybrid environment between the maternal and fetal vascular components. It is tempting to speculate that some aspect of early trophoblast biology (proliferation, differentiation, migration, or function) becomes compromised with Rybp deficiency, as has been described previously for other knockout mice (reviewed in references 4 and 25). Defective trophoblasts may explain why the *rybp*$^{-/-}$ embryos are unable to trigger full decidualization in vivo, as evidenced by the lack of apoptotic response following the initiation of implantation (Fig. 3). In turn, failed decidualization may provide the basis for the developmental arrest as well, although we cannot rule out that there also may be an inherent defect in the epiblast. Future studies can address whether the early defect is primarily extraembryonic in nature, and, if so, whether and how trophoblasts may be affected. Of note, several of the Polycomb group (PcG) repressors have been shown to function in the trophectoderm and its derivatives, as well as in the process of imprinted X inactivation that occurs therein (6, 8, 20, 32). Included among these is the Ring1B PcG protein that is a verified binding protein for both Rybp and Yaf2 (9, 15).

Beyond the role of Rybp function in the implanting embryo, Rybp function is suggested by our findings to be crucial for normal CNS development. These findings were made possible by the fact that the early lethal effect of Rybp deficiency was overcome in the context of our heterozygous null or chimeric mice. The CNS defect in the heterozygotes manifests as exencephaly in part due to defective neural tube closure (Fig. 6i to p), suggesting that this process is sensitive to changes in Rybp abundance. The variable penetrance of this defect in the *rybp* heterozygotes may indicate that expression and/or function of the retained wild-type *rybp* allele is being modified differentially in affected or nonaffected animals. This is also supported by the observation that the penetrance of the exencephaly was influenced by genetic background, rising with increased 129Sv and decreased CD1 genome contribution (data not shown). It is important to note that exencephaly is a common phenotype in genetically engineered mice (most often reported for homozygous null animals) (for reviews, see references 3 and 12) and has sometimes been classified as a mere indicator of a moribund or compromised animal. However, the additional fact that the CNS is the organ that selectively suffers the consequences of Rybp deficiency in our chimeric animals suggests a more specific role for Rybp therein. In the chimeras, the presence of Rybp-deficient cells during the course of CNS development resulted in chaotic forebrain overgrowth, among other cephalic abnormalities, including some degree of neural tube openness (Fig. 6c to h). Clues as to why the overgrowth occurs may be derived from Rybp's expression profile in the developing cerebral cortex, wherein Rybp appears to be expressed more in postmitotic neurons (Fig. 7e to i); this may indicate a role for Rybp in cell cycle exit or the commitment to differentiation.

With respect to open neural tube defects (NTDs), disruption in the balance of neuroepithelial cell proliferation/differentiation is a known cause. Other cellular processes involved in neural tube closure include proliferation/expansion of the cranial mesenchyme, cytoskeletal reorganization, neural crest migration, and neuroepithelial cell death (for reviews, see references 3 and 12). While numerous transcriptional regulators have been tied to NTD etiology, PcG proteins have not yet been implicated (although YY1 is a possible exception; see reference 7). However, a recent study has shown that the antiepileptic drug valproic acid, a potent teratogen and inducer of NTDs in mice and humans, can affect PcG gene expression, at least in the context of the axial skeleton (23). As such, the NTDs we observed could reflect a role for Rybp in PcG protein-mediated silencing of genes controlling neuronal survival, differentiation, or migration. It is also worth noting that the CNS phenotype observed in our heterozygous animals is reminiscent of that reported previously for mice homozygous null for the proapoptotic factor *caspase 9*, *caspase 3*, or *apaf1* (see reference 17 and the references therein). Specifically, these null embryos develop exencephaly due to perturbed apoptosis as well as increased proliferation of immature neurons and precursor cells of the forebrain (see reference 17 and the references therein). The similarity to the *rybp* CNS phenotype (in both the heterozygotes and the chimeras) could be pursued further, given (i) the published roles of Rybp in interacting with components of the death receptor pathway (33) and (ii) our finding of an impaired apoptotic response triggered by implanting *rybp*$^{-/-}$ conceptuses (see above and Fig. 3).

On a final note, several other knockout mice have been reported to exhibit phenotypes similar to those resulting from Rybp deficiency, namely lethality around the time of implantation for the homozygotes and exencephaly for a subset of the heterozygotes. Among the genes manipulated in those mice are transcription factors such as YY1 (7) and chromatin remodeling factors such as Brg1 (2) and Srg3 (16). It is of interest that these factors, as well as Rybp, have the potential to affect numerous downstream gene targets, this perhaps being the basis for the complex phenotypes seen in the engineered mice. The cells and mice we have generated may allow us to assess the potential relationships between Rybp and these proteins and to place Rybp within known genetic networks. These tools also will provide opportunities for the elucidation of the precise molecular roles of Rybp as they relate to transcriptional regulation, apoptosis, and/or yet-to-be-identified cellular processes. In the future, the generation of conditional or tissue-specific knockout mice, with the CNS being an attractive focus, will allow us to understand more about Rybp's biological roles during development and in the context of aging and disease.

ACKNOWLEDGMENTS

We thank Kat Hadjantonakis, Virginia Papaioannou, Jean Hebert, Rod Bronson, Bernice Morrow, and Ales Cvekl, as well as members of the Schreiber-Agus laboratory, for stimulating discussions and critical reading of the manuscript. We are indebted to Radma Mahmood, Harry Hou, Jing Ruan, and Jiu-feng Li for superb technical assistance.

This work was supported in part by Public Health Service grants CA92558 (N.S.-A.) and CA68440, CA76354, and CA104292 (J.L.) from the National Cancer Institute. Funds from the New York Speaker's Fund for Biomedical Research (N.S.-A.) and support from the Albert Einstein Cancer Center (N.S.-A. and J.L.) are acknowledged as well.

REFERENCES

1. **Atchison, L., A. Ghias, F. Wilkinson, N. Bonini, and M. L. Atchison.** 2003. Transcription factor YY1 functions as a PcG protein in vivo. EMBO J. **22:**1347–1358.
2. **Bultman, S., T. Gebuhr, D. Yee, C. La Mantia, J. Nicholson, A. Gilliam, F. Randazzo, D. Metzger, P. Chambon, G. Crabtree, and T. Magnuson.** 2000. A Brg1 null mutation in the mouse reveals functional differences among mammalian SWI/SNF complexes. Mol. Cell **6:**1287–1295.
3. **Copp, A. J., N. D. Greene, and J. N. Murdoch.** 2003. The genetic basis of mammalian neurulation. Nat. Rev. Genet. **4:**784–793.
4. **Cross, J. C.** 2000. Genetic insights into trophoblast differentiation and placental morphogenesis. Semin. Cell Dev. Biol. **11:**105–113.
5. **Danen-Van Oorschot, A. A., P. Voskamp, M. C. Seelen, M. H. Van Miltenburg, M. W. Bolk, S. W. Tait, J. G. Boesen-De Cock, J. L. Rohn, J. Borst, and M. H. Noteborn.** 2004. Human death effector domain-associated factor interacts with the viral apoptosis agonist Apoptin and exerts tumor-preferential cell killing. Cell Death Differ.
6. **de Napoles, M., J. E. Mermoud, R. Wakao, Y. A. Tang, M. Endoh, R. Appanah, T. B. Nesterova, J. Silva, A. P. Otte, M. Vidal, H. Koseki, and N. Brockdorff.** 2004. Polycomb group proteins Ring1A/B link ubiquitylation of histone H2A to heritable gene silencing and X inactivation. Dev. Cell **7:**663–676.
7. **Donohoe, M. E., X. Zhang, L. McGinnis, J. Biggers, E. Li, and Y. Shi.** 1999. Targeted disruption of mouse Yin Yang 1 transcription factor results in peri-implantation lethality. Mol. Cell. Biol. **19:**7237–7244.
8. **Fang, J., T. Chen, B. Chadwick, E. Li, and Y. Zhang.** 2004. Ring1b-mediated H2A ubiquitination associates with inactive X chromosomes and is involved in initiation of X inactivation. J. Biol. Chem. **279:**52812–52815.
9. **Garcia, E., C. Marcos-Gutierrez, M. del Mar Lorente, J. C. Moreno, and M. Vidal.** 1999. RYBP, a new repressor protein that interacts with components of the mammalian Polycomb complex, and with the transcription factor YY1. EMBO J. **18:**3404–3418.
10. **Hatten, M. E.** 1999. Central nervous system neuronal migration. Annu. Rev. Neurosci. **22:**511–539.
11. **Joswig, A., H. D. Gabriel, M. Kibschull, and E. Winterhager.** 2003. Apoptosis in uterine epithelium and decidua in response to implantation: evidence for two different pathways. Reprod. Biol. Endocrinol. **1:**44.
12. **Juriloff, D. M., and M. J. Harris.** 2000. Mouse models for neural tube closure defects. Hum. Mol. Genet. **9:**993–1000.
13. **Jurisicova, A., S. Varmuza, and R. F. Casper.** 1996. Programmed cell death and human embryo fragmentation. Mol. Hum. Reprod. **2:**93–98.
14. **Kalenik, J. L., D. Chen, M. E. Bradley, S. J. Chen, and T. C. Lee.** 1997. Yeast two-hybrid cloning of a novel zinc finger protein that interacts with the multifunctional transcription factor YY1. Nucleic Acids Res. **25:**843–849.
15. **Kaneko, T., H. Miyagishima, T. Hasegawa, Y. Mizutani-Koseki, K. Isono, and H. Koseki.** 2003. The mouse YAF2 gene generates two distinct transcripts and is expressed in pre-and postimplantation embryos. Gene **315:** 183–192.
16. **Kim, J. K., S. O. Huh, H. Choi, K. S. Lee, D. Shin, C. Lee, J. S. Nam, H. Kim, H. Chung, H. W. Lee, S. D. Park, and R. H. Seong.** 2001. Srg3, a mouse homolog of yeast SWI3, is essential for early embryogenesis and involved in brain development. Mol. Cell. Biol. **21:**7787–7795.
17. **Lossi, L., and A. Merighi.** 2003. In vivo cellular and molecular mechanisms of neuronal apoptosis in the mammalian CNS. Prog. Neurobiol. **69:**287–312.
18. **Lund, A. H., and M. van Lohuizen.** 2004. Polycomb complexes and silencing mechanisms. Curr. Opin. Cell Biol. **16:**239–246.
19. **Madge, B., C. Geisen, T. Moroy, and M. Schwab.** 2003. Yaf2 inhibits Myc biological function. Cancer Lett. **193:**171–176.
20. **Mak, W., J. Baxter, J. Silva, A. E. Newall, A. P. Otte, and N. Brockdorff.** 2002. Mitotically stable association of polycomb group proteins Eed and Enx1 with the inactive X chromosome in trophoblast stem cells. Curr. Biol. **12:**1016–1020.
21. **Nagy, A., J. Rossant, R. Nagy, W. Abramow-Newerly, and J. C. Roder.** 1993. Derivation of completely cell culture-derived mice from early-passage embryonic stem cells. Proc. Natl. Acad. Sci. USA **90:**8424–8428.
22. **Ogawa, H., K. Ishiguro, S. Gaubatz, D. M. Livingston, and Y. Nakatani.** 2002. A complex with chromatin modifiers that occupies E2F- and Myc-responsive genes in G0 cells. Science **296:**1132–1136.
23. **Okada, A., Y. Aoki, K. Kushima, H. Kurihara, M. Bialer, and M. Fujiwara.** 2004. Polycomb homologs are involved in teratogenicity of valproic acid in mice. Birth Defects Res. A **70:**870–879.
24. **Pirity, M., A. K. Hadjantonakis, and A. Nagy.** 1998. Embryonic stem cells, creating transgenic animals. Methods Cell Biol. **57:**279–293.
25. **Rossant, J., and J. C. Cross.** 2001. Placental development: lessons from mouse mutants. Nat. Rev. Genet. **2:**538–548.
26. **Sauer, B., and N. Henderson.** 1990. Targeted insertion of exogenous DNA into the eukaryotic genome by the Cre recombinase. New Biol. **2:**441–449.
27. **Sawa, C., T. Yoshikawa, F. Matsuda-Suzuki, S. Delehouzee, M. Goto, H. Watanabe, J. Sawada, K. Kataoka, and H. Handa.** 2002. YEAF1/RYBP and YAF-2 are functionally distinct members of a cofactor family for the YY1 and E4TF1/hGABP transcription factors. J. Biol. Chem. **277:**22484–22490.
28. **Schlisio, S., T. Halperin, M. Vidal, and J. R. Nevins.** 2002. Interaction of YY1 with E2Fs, mediated by RYBP, provides a mechanism for specificity of E2F function. EMBO J. **21:**5775–5786.
29. **Tam, P. P., and J. Rossant.** 2003. Mouse embryonic chimeras: tools for studying mammalian development. Development **130:**6155–6163.
30. **Trimarchi, J. M., B. Fairchild, J. Wen, and J. A. Lees.** 2001. The E2F6 transcription factor is a component of the mammalian Bmi1-containing polycomb complex. Proc. Natl. Acad. Sci. USA **98:**1519–1524.
31. **Wang, H., L. Wang, H. Erdjument-Bromage, M. Vidal, P. Tempst, R. S. Jones, and Y. Zhang.** 2004. Role of histone H2A ubiquitination in Polycomb silencing. Nature **431:**873–878.
32. **Wang, J., J. Mager, Y. Chen, E. Schneider, J. C. Cross, A. Nagy, and T. Magnuson.** 2001. Imprinted X inactivation maintained by a mouse Polycomb group gene. Nat. Genet. **28:**371–375.
33. **Zheng, L., O. Schickling, M. E. Peter, and M. J. Lenardo.** 2001. The death effector domain-associated factor plays distinct regulatory roles in the nucleus and cytoplasm. J. Biol. Chem. **276:**31945–31952.